Electronic Supplementary Material (ESI) for Journal of Materials Chemistry C.

Supporting Information

Molecular Isomeric Engineering of Naphtylquinoline-Containing Dinuclear Platinum Complexes to Tune Emission from Deep Red to Near Infrared

Wenjing Xiong,[a,b] Fanyuan Meng,[a,c] Caifa You,[a] Pu Wang,[a] Junting Yu,[d] Xiugang Wu[b], Yong Pei,[a] Yafei Wang,[b] Shijian Su*[c] and Weiguo Zhu*[a,b]*

Contents

(2nq)$_2$Pt$_2$(μ-OXT)$_2$ (c).

Figure S13. MALDI-TOF MS plots of (niq)$_2$Pt$_2$(μ-OXT)$_2$ (a) , (nq)$_2$Pt$_2$(μ-OXT)$_2$ (b) and (2nq)$_2$Pt$_2$(μ-OXT)$_2$ (c).

Table S1. Calculated excitation energy (E), oscillator strength (f), dominant contributing transitions and associated percent contribution and assignment of complexes (niq)$_2$Pt$_2$(μ-OXT)$_2$, (nq)$_2$Pt$_2$(μ-OXT)$_2$ and (2nq)$_2$Pt$_2$(μ-OXT)$_2$ (c).

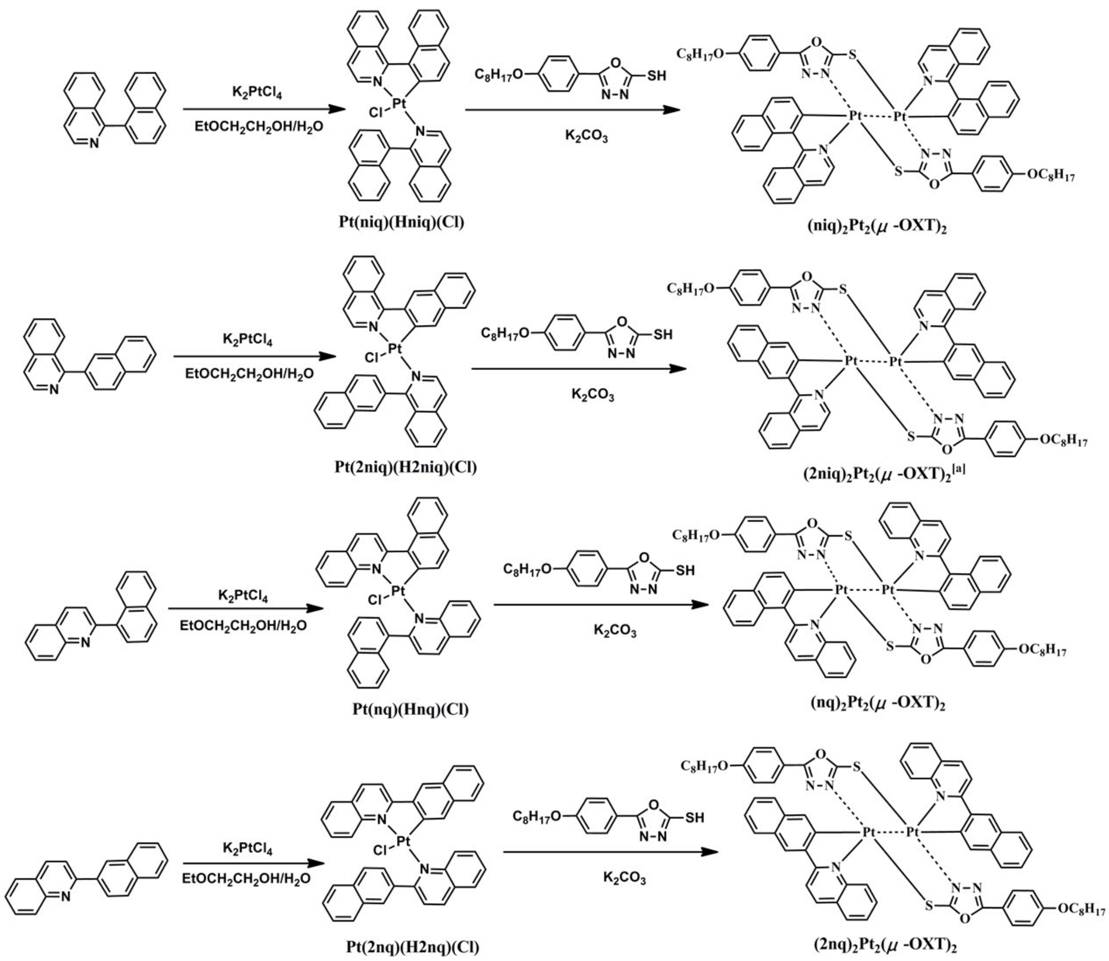

[a] Cited from J. Mater. Chem. C, 2016, 4, 6007.

Figure S1. The synthetic routes of dinuclear platinum complexes.

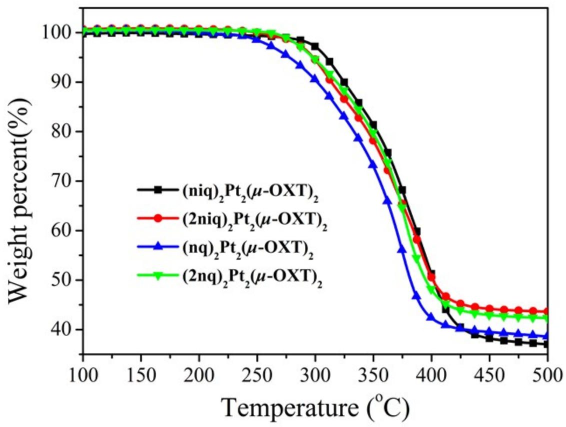

Figure S2. TGA curves of dinuclear platinum complexes.

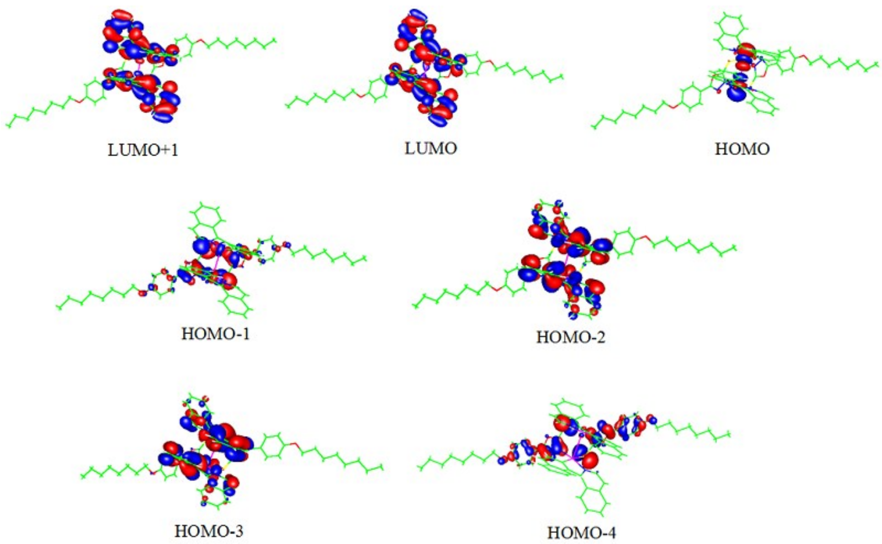

Figure S3. Representative frontier orbitals for $(niq)_2Pt_2(\mu\text{-}OXT)_2$.

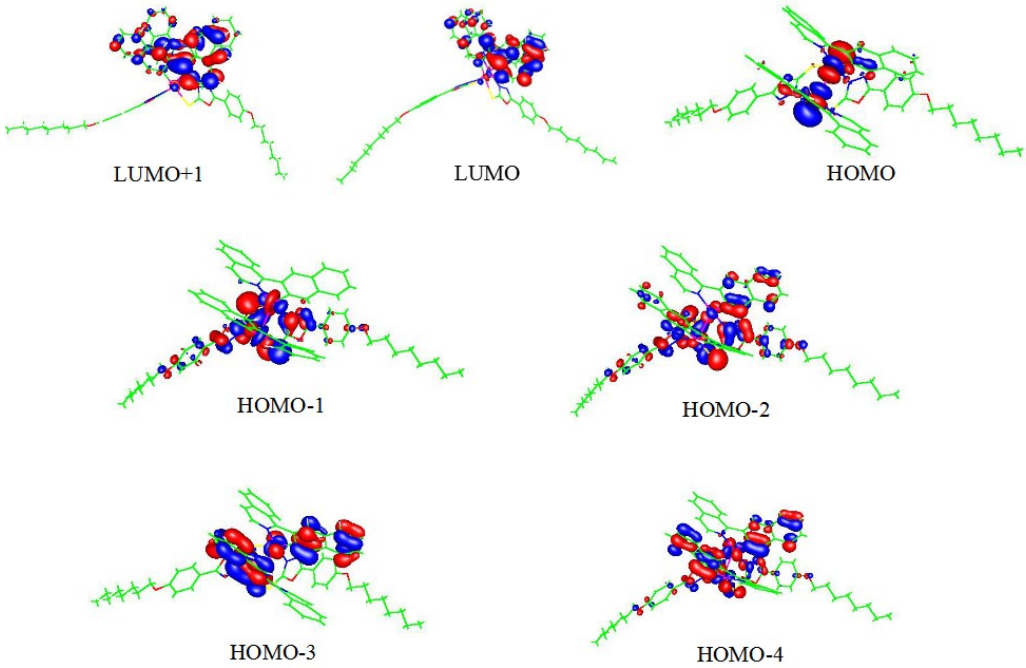

Figure S4. Representative frontier orbitals for $(2niq)_2Pt_2(\mu\text{-}OXT)_2$.

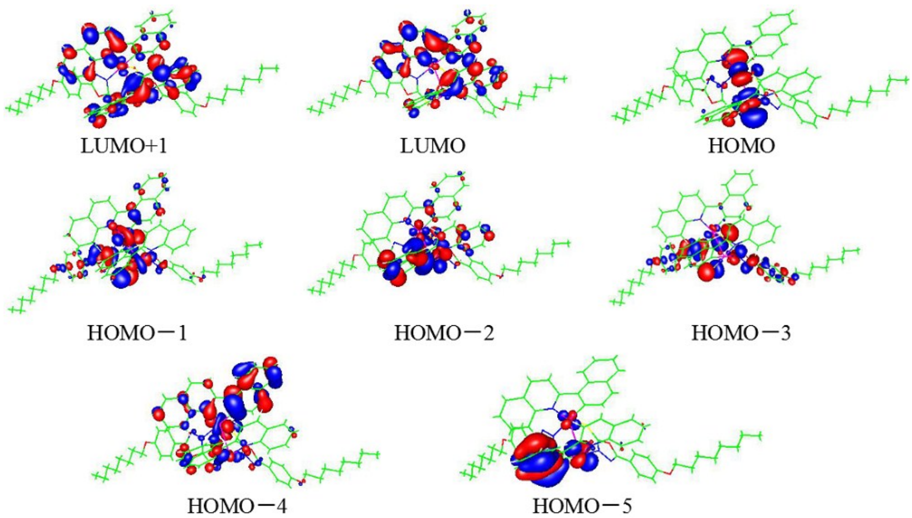

Figure S5. Representative frontier orbitals for $(nq)_2Pt_2(\mu\text{-}OXT)_2$.

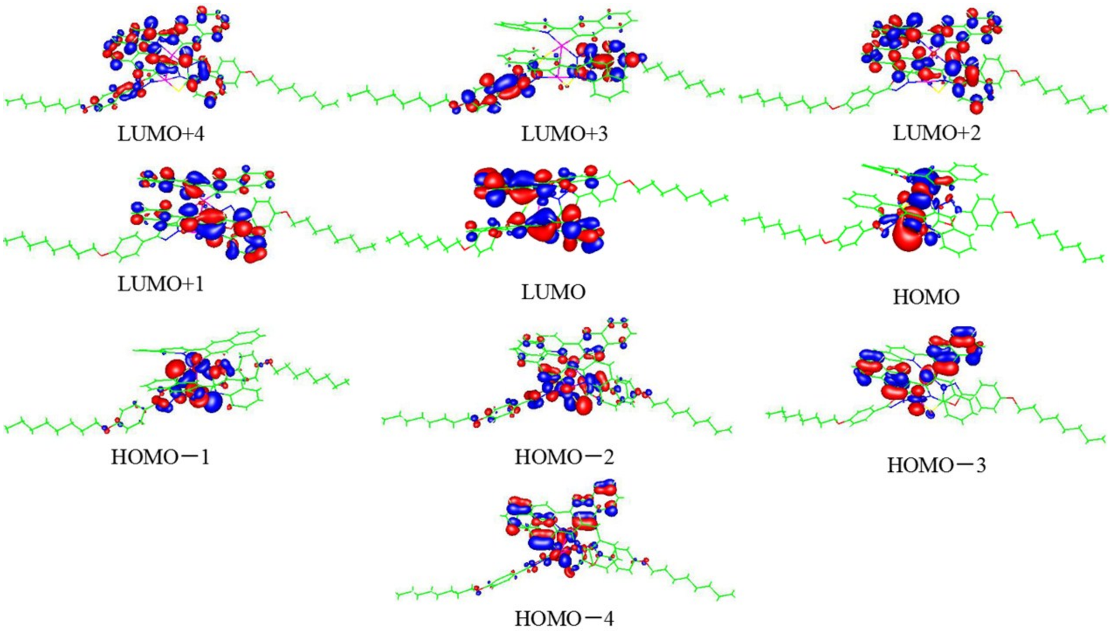

Figure S6. Representative frontier orbitals for $(2nq)_2Pt_2(\mu\text{-OXT})_2$.

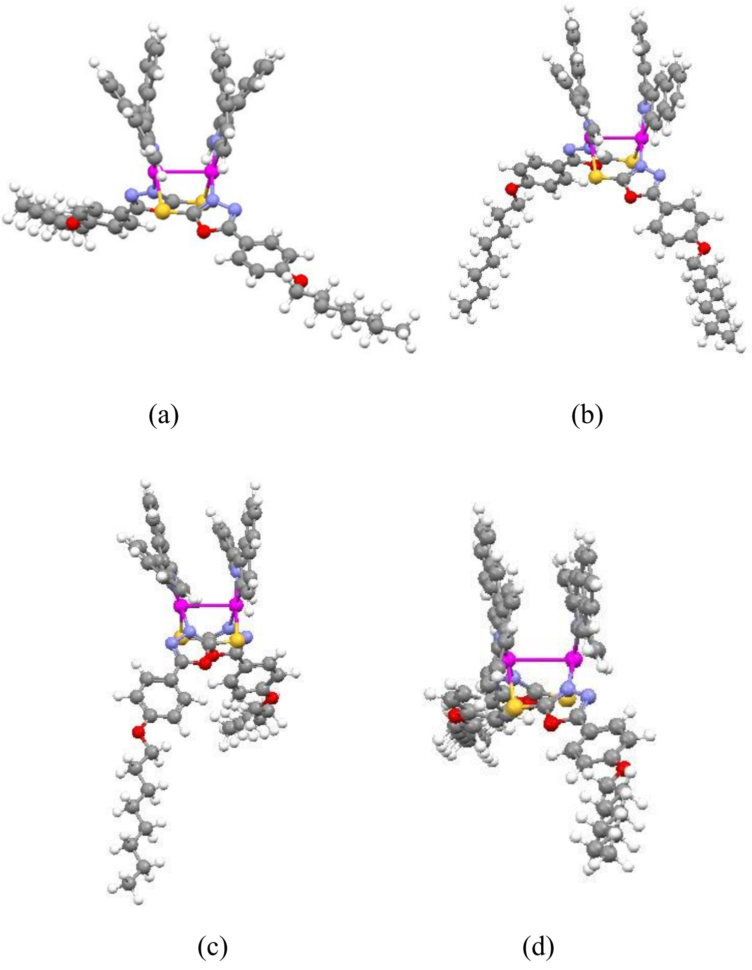

Figure S7. Optimal structure of $(niq)_2Pt_2(\mu\text{-OXT})_2$ (a), $(2niq)_2Pt_2(\mu\text{-OXT})_2$ (b), $(nq)_2Pt_2(\mu\text{-OXT})_2$ (c) and $(2nq)_2Pt_2(\mu\text{-OXT})_2$ (d). Selected dihedral angles: (a) N2-C3-C11-C12: 26.48°, N44-C45-

C53- C54: 26.74°; (b) N2-C3-C7-C8: 10.51°, N40-C41-C45-C46: 9.98°; (c) N2-C3-C6-C7: 22.66°, N39-C40-C44-C45: 24.78°; (d) N2-C3-C7-C8: 14.92°, N40-C41-C45- C46: 16.55°.

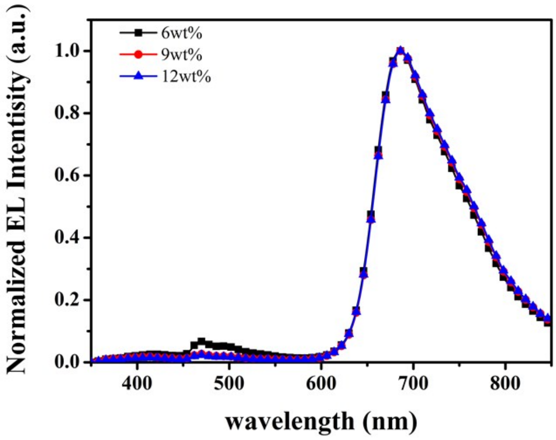

（A）

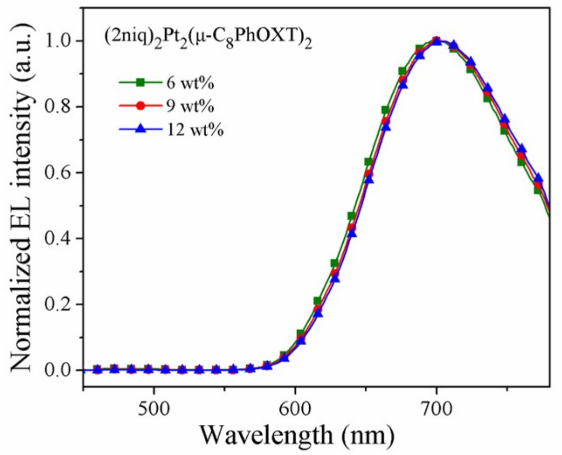

(B)

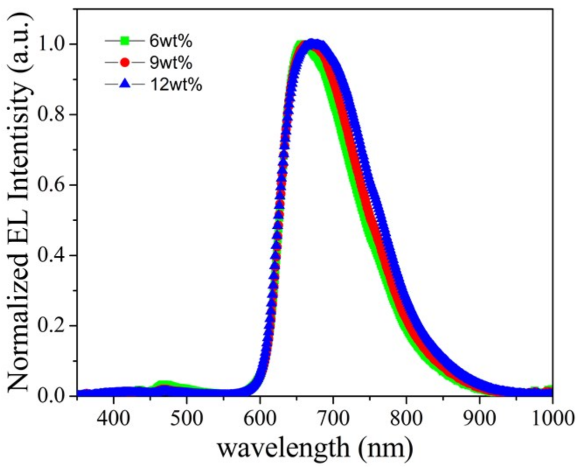

(C)

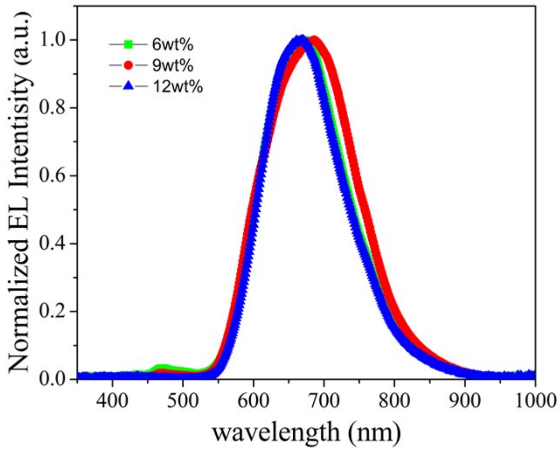

(D)

Figure S8. EL spectra of the devices of A, B, C and D at different dopant concentrations from 6 wt% and 9 wt% to 12 wt%.

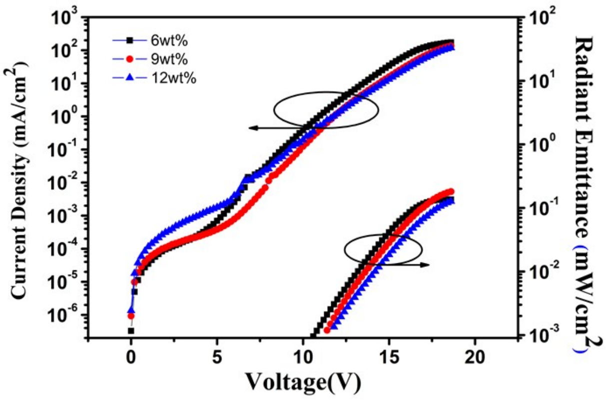

(A)

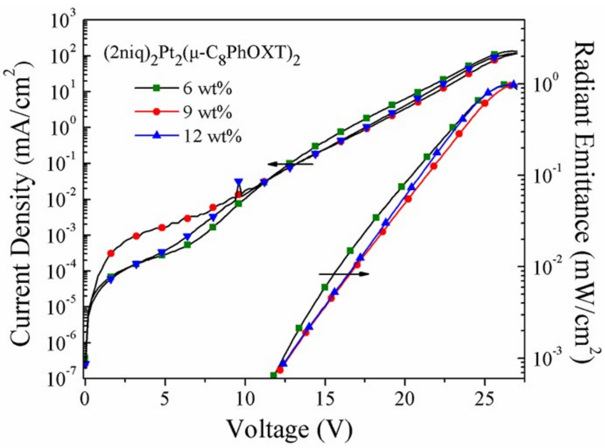

(B)

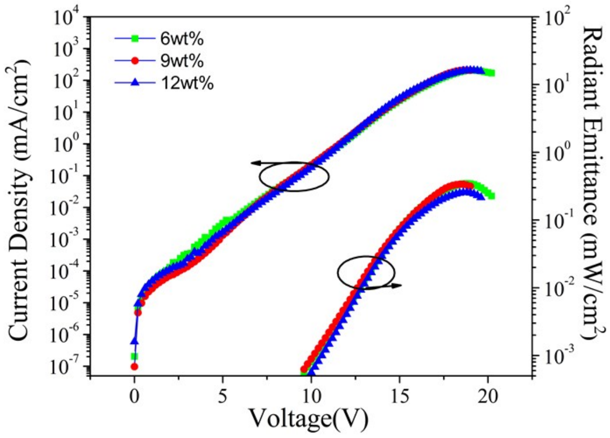

(C)

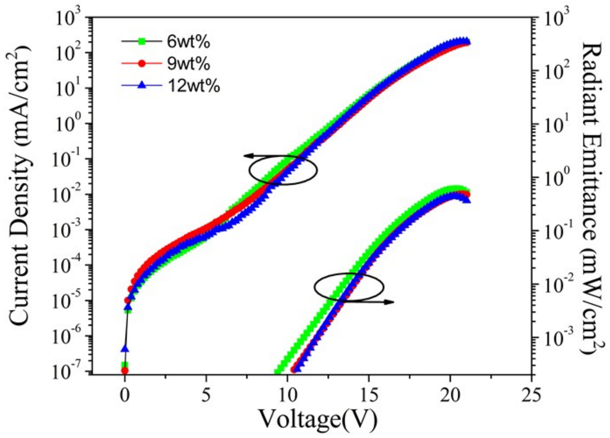

(D)

Figure S9. The J-V-R curves of the the devices A, B, C and D at different dopant concentrations from 6 wt% and 9 wt% to 12 wt%.

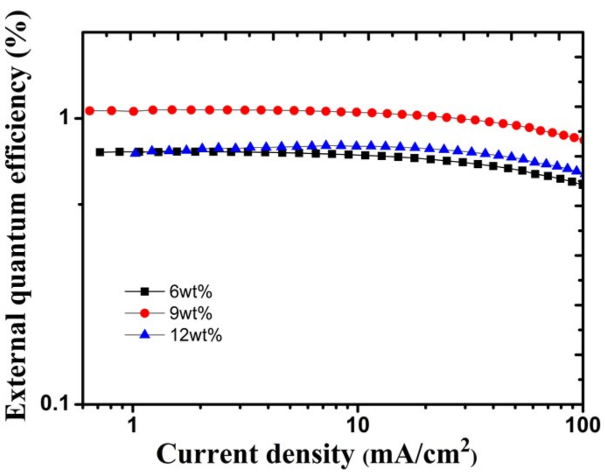

(A)

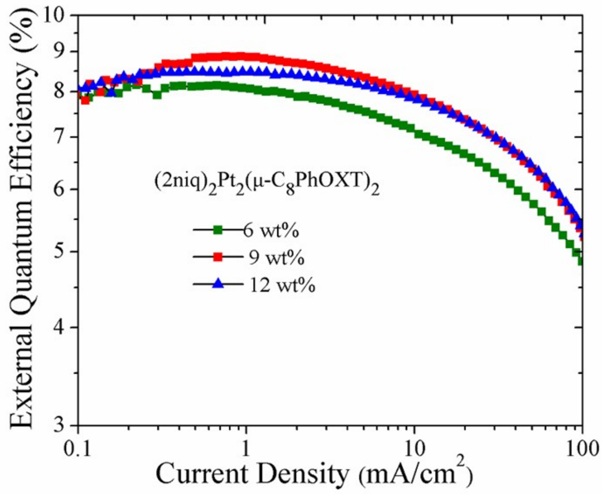

External Quantum Efficiency (%)
Current Density (mA/cm^2)
$(2niq)_2Pt_2(\mu\text{-}C_8PhOXT)_2$
6 wt%
9 wt%
12 wt%

(B)

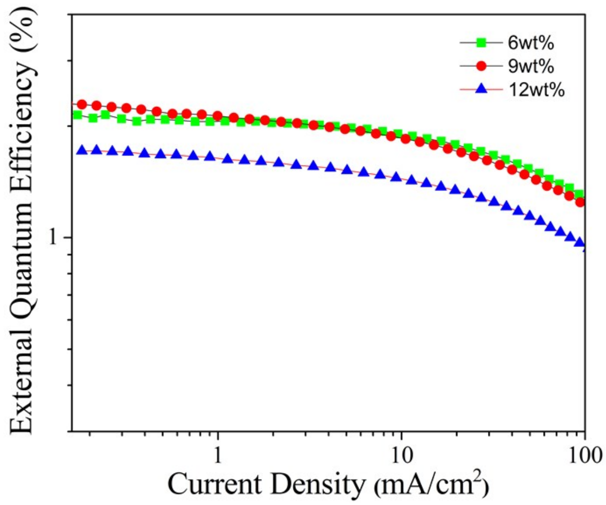

External Quantum Efficiency (%)
Current Density (mA/cm^2)
6wt%
9wt%
12wt%

(C)

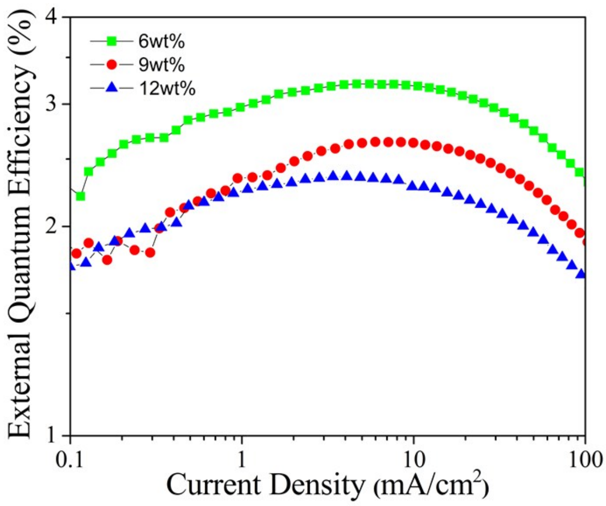

External Quantum Efficiency (%)
Current Density (mA/cm^2)
6wt%
9wt%
12wt%

(D)

Figure S10. *EQE-J* curves of the devices of A, B, C and D at different dopant concentrations from 6 wt% and 9 wt% to 12 wt%.

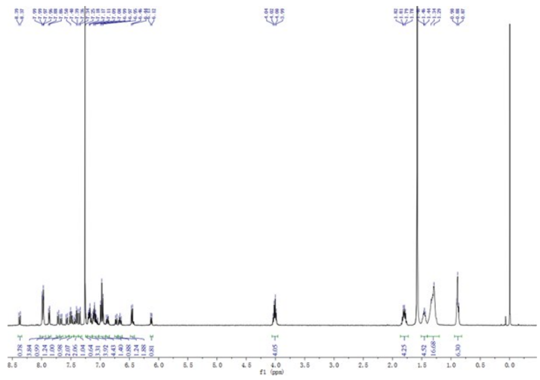

(a)

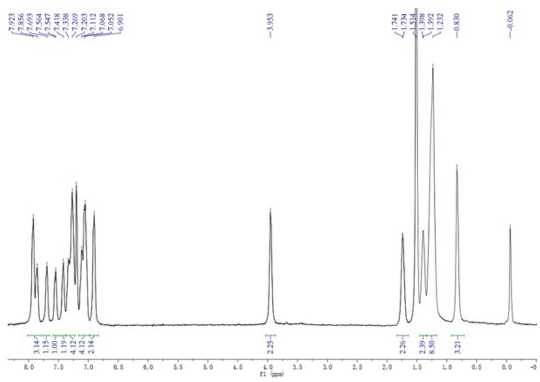

(b)

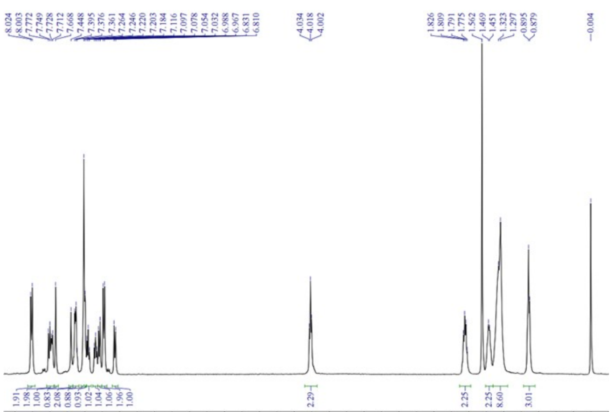

(c)

Figure S11. ^{1}H NMR of $(niq)_2Pt_2(\mu\text{-}OXT)_2$ (a), $(nq)_2Pt_2(\mu\text{-}OXT)_2$ (b) and $(2nq)_2Pt_2(\mu\text{-}OXT)_2$ (c).

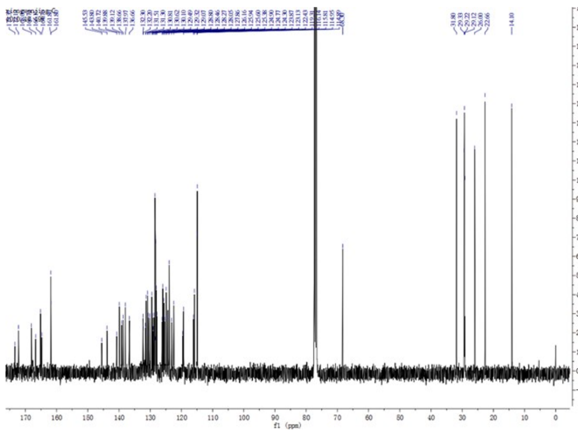

(a)

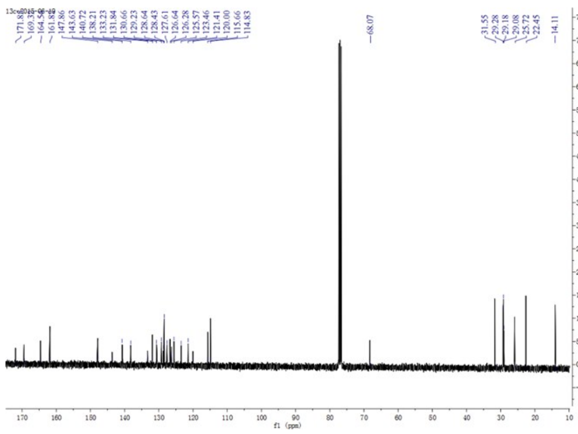

(b)

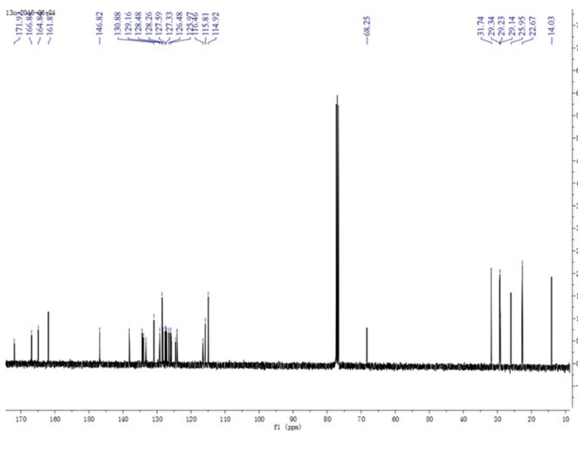

(c)

Figure S12. ^{13}C NMR of $(niq)_2Pt_2(\mu\text{-}OXT)_2$ (a) , $(nq)_2Pt_2(\mu\text{-}OXT)_2$ (b) and $(2nq)_2Pt_2(\mu\text{-}OXT)_2$ (c).

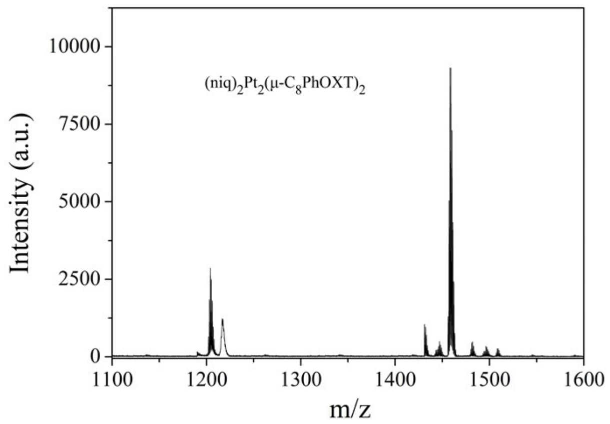

(a)

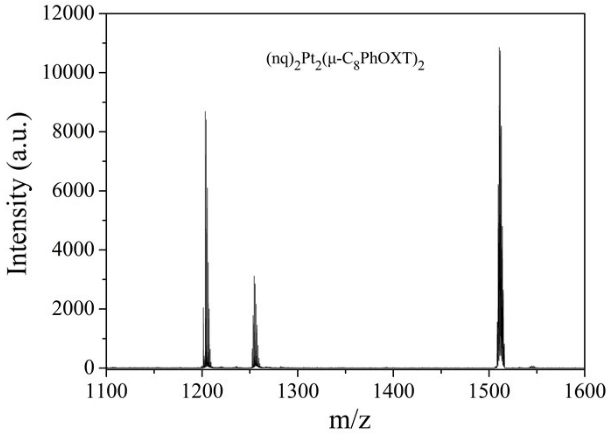

(b)

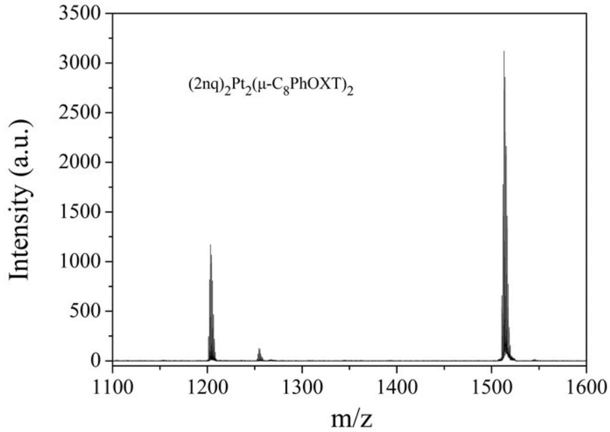

(c)

Figure S13. MALDI-TOF MS plots of (niq)$_2$Pt$_2$(μ-OXT)$_2$ (a) , (nq)$_2$Pt$_2$(μ-OXT)$_2$ (b) and (2nq)$_2$Pt$_2$(μ-OXT)$_2$ (c).

Table S1. Calculated excitation energy (E), oscillator strength (f), dominant contributing transitions and associated percent contribution and assignment of complexes (niq)$_2$Pt$_2$(μ-OXT)$_2$,

$(nq)_2Pt_2(\mu\text{-}OXT)_2$ and $(2nq)_2Pt_2(\mu\text{-}OXT)_2$ (c).[a]

complexes	S_n	E/eV	E/nm	f	dominant transitions (percent contribution[b])	assignment
$(niq)_2Pt_2(\mu\text{-}OXT)_2$	1	2.73	454.2	0.034	HOMO → LUMO (98.7%)	MMLCT
	2	2.94	421.8	0.003	HOMO → LUMO+1 (97.9%)	MMLCT
	3	2.91	426.1	0.002	HOMO –1 → LUMO (98.4%)	MLLCT
	4	3.05	406.6	0.001	HOMO –2 → LUMO (93.9%)	ILCT
	5	3.08	402.6	0.089	HOMO –3 → LUMO (87.0%)	ILCT
	6	3.12	397.4	0.0004	HOMO –1 → LUMO+1 (94.3%)	LLCT
	7	3.13	396.2	0.018	HOMO –4 → LUMO (95.3%)	LLCT
	8	3.26	380.4	0.040	HOMO –2 → LUMO+1 (94.6%)	ILCT
	9	3.29	376.9	0.001	HOMO –3 → LUMO+1 (94.2%)	ILCT
	10	3.34	371.3	0.007	HOMO –4 → LUMO+1 (98.1%)	LLCT
$(nq)_2Pt_2(\mu\text{-}OXT)_2$	1	2.80	442.8	0.025	HOMO → LUMO (92.3%)	MMLCT
	2	2.91	426.1	0.015	HOMO → LUMO+1 (89.3%)	MMLCT
					HOMO –3 → LUMO+1 (3.4%)	LLCT
	3	2.90	428.2	0.016	HOMO –1 → LUMO (89.9%)	MMLCT
					HOMO → LUMO (3.5%)	MMLCT
	4	3.01	412.2	0.011	HOMO –1 → LUMO+1 (79.3%)	MMLCT
					HOMO –3 → LUMO (5.5%)	LLCT
					HOMO –2 → LUMO (5.5%)	LLCT
	6	3.08	402.6	0.003	HOMO –3 → LUMO (59.7%)	LLCT
					HOMO –2 → LUMO (28.7%)	LLCT
					HOMO –2 → LUMO+1 (3.5%)	LLCT
	9	3.17	391.2	0.038	HOMO –3 → LUMO+1 (78.5%)	LLCT

					HOMO –2 → LUMO+1 (10.8%)	LLCT
					HOMO –1 → LUMO+1 (4.2%)	LLCT
	10	3.48	356.3	0.011	HOMO –4 → LUMO (93.6%)	ILCT
	11	4.00	310.0	0.024	HOMO –5 → LUMO (91.2%)	LLCT
$(2nq)_2Pt_2(\mu\text{-}OXT)_2$	1	2.63	471.5	0.001	HOMO –1 → LUMO (65.9%)	MMLCT
					HOMO → LUMO (26.0%)	MMLCT
	2	2.66	466.2	0.009	HOMO–1 → LUMO+1 (76.5%)	MMLCT
					HOMO → LUMO+1 (15.9%)	MMLCT
	3	2.78	446.0	0.007	HOMO → LUMO (70.1%)	MMLCT
					HOMO –1 → LUMO (28.3%)	MMLCT
	4	2.83	438.2	0.004	HOMO → LUMO+1 (80.9%)	MMLCT
					HOMO –1 → LUMO+1 (16.9%)	LLCT
	5	2.97	417.8	0.002	HOMO –2 → LUMO (89.9%)	LLCT
					HOMO –4 → LUMO (4.8%)	LLCT
	6	3.14	394.9	0.029	HOMO –2 → LUMO+1 (87.7%)	LLCT
					HOMO –4 → LUMO+1 (6.6%)	LLCT
	11	3.47	357.3	0.005	HOMO –1 → LUMO+2 (69.1%)	LLCT
					HOMO → LUMO+2 (27.9%)	MMLCT
	21	3.84	322.9	0.004	HOMO –1 → LUMO+3 (66.6%)	ILCT
					HOMO → LUMO+4 (21.3%)	MMLCT
					HOMO –1 → LUMO+4 (4.0%)	LLCT
	32	4.09	303.2	0.246	HOMO –2 → LUMO+3 (88.8%)	ILCT
					HOMO –2 → LUMO+4 (3.7%)	LLCT

[a] Computed at the DFT/B3LYP/def-tzvp. [b] The actual percent contribution = (configuration coefficient)$^2 \times 2 \times 100\%$